Design, Development, and Operation of a Low-Intensity Focused Ultrasound Pulsation (LIFUP) System for Clinical Use

Mark E. Schafer, *Senior Member, IEEE*, Norman M. Spivak, Alexander S. Korb, and Alexander Bystritsky

***Abstract*— Noninvasive low-intensity focused ultrasound pulsation (LIFUP) neuromodulation provides a unique approach to both investigating and treating the brain. This work describes a well-calibrated, simple-to-use ultrasound stimulation system for neuromodulation studies. It provides a single-element 650-kHz transducer design and a straightforward control mechanism, with extensive calibration and internal electronic monitoring to prevent unwanted over or under treatment. One goal of this approach is to relieve researchers of many of the details associated with developing their own exposure equipment. A unique transducer positioning system and distinctive MRI fiducial targets simplify alignment and targeting. The system design, control software, calibration, and alignment techniques are described in detail. Examples of transducer targeting and neurostimulation using the system are provided.**

***Index Terms*— Low intensity focused ultrasound pulsation (LIFUP), low intensity focused ultrasound (LIFU), neuromodulation, transducer, ultrasound.**

I. Background

FOCUSED ultrasound is a means of delivering mechanical energy to tissue. The concept of using sound waves to modulate the neuronal activity has been under investigation since 1958 [1]. Since then, the neuromodulatory effects of focused ultrasound have been demonstrated numerous times in multiple animal models [2], [3]. Animal studies of focused ultrasound have shown that it is capable of various forms of neuromodulation including stimulating auditory nerve responses [4], down-regulating nervous conduction [5], and inducing reproducible excitation of neuronal circuits in the motor cortex in excised rodent brain [6] and in live animals [7].

Noninvasive low-intensity focused ultrasound pulsation (LIFUP) modulates neural activity in the human brain [3] using intensities that do not cause substantial tissue heating or irreversible tissue effects. In one study, LIFUP targeted on the hand area of the somatosensory cortex elicited both tactile sensation in the contralateral hand and relevant EEG evoked potentials [8]. In another set of studies targeting the same region during concurrent median nerve stimulation, LIFUP significantly decreased the amplitude of stimulus-evoked potentials [9] and altered the dynamics of intrinsic EEG activity [10]. This study showed that LIFUP can not only modulate the brain electrical activity but also affect perceptions and behavior.

The low energy of LIFUP falls below the threshold to induce tissue damage, often with intensities that are near or below those used in diagnostic ultrasound. The safety of focused ultrasound has been assessed in multiple experiments. In sharp contrast to high-intensity focused ultrasound, none of the studies using LIFUP suggest any adverse effects from histological, blood–brain barrier or behavioral data. In general, any potential ultrasound-induced tissue damage appears to be caused primarily by heating, and an increase in temperature is not required to exert effects on neural activity [7], [11]. Several studies looked thoroughly for evidence of damage caused by LIFUP and found none [6], [7], [12], [13]. Even with chronic stimulation of LIFUP for 48 h, no alterations were seen in the fine structure of neuronal membranes [6].

More detailed information regarding the safety of focused ultrasound can be found in recent review articles [2], [3], [14]–[16].

For clinical application, LIFUP has demonstrated the ability to safely modulate the neural activity in humans and in animal models [2], [3] and is compatible with functional magnetic resonance imaging (fMRI) technology [12], [17], [18]. LIFUP involves passing low-energy pulsed sound waves through the skin and skull, typically through the temporal region. This region, often referred to as the "temporal window," is generally thinner and flatter than other locations on the skull, and transcranial Doppler (TCD) assessment of blood flow within the

Manuscript received March 25, 2020; accepted June 28, 2020. Date of publication July 2, 2020; date of current version December 23, 2020. Supported in part by Brainsonix Corporation, Pacific Institute of Medical Research and Tiny Blue Dot Foundation. *(Corresponding author: Mark E. Schafer.)*

Mark E. Schafer is with Brainsonix, Inc., LosAngeles, CA 91403 USA, and also with Sonic Tech, Inc., Ambler, PA 19002 USA (e-mail: mark@brainsonix.com).

Norman M. Spivak is with the Department of Neurosurgery, University of California at Los Angeles, Los Angeles, CA 90095 USA, and also with the Department of Psychiatry and Biobehavioral Sciences, University of California at Los Angeles, Los Angeles, CA 90095 USA (e-mail: nspivak@mednet.ucla.edu).

Alexander S. Korb is with the Department of Psychiatry and Biobehavioral Science, University of California at Los Angeles, Los Angeles, CA 90095 USA, and also with Brainsonix, Inc., Los Angeles, CA 91403 USA (e-mail: alexk@brainsonix.com).

Alexander Bystritsky is with Brainsonix, Inc., Los Angeles, CA 91403 USA, and also with the Department of Psychiatry and Biobehavioral Science, University of California at Los Angeles, Los Angeles, CA 90095 USA (e-mail: sasha@brainsonix.com).

Digital Object Identifier 10.1109/TUFFC.2020.3006781

brain is usually conducted through the temporal window [19]. TCD systems typically operate at 2 MHz, and the attenuation and beam distortion effects of the skull have been studied for a number of years [20], [21]. At a LIFUP operating frequency of 650 kHz, less of the ultrasound energy is absorbed by the skull, and the shape of the focal region is better preserved (see Section IV-B) [22]. Thus, the ultrasound wave can be focused with precision in three dimensions within the brain. While this focal volume is small relative to the size of the brain (<0.2 cm^3 or approximately 0.01% of the total brain volume), it can potentially stimulate tens of thousands of neurons within the focal region. This is an acceptable stimulation level for producing fMRI signals that can inform scientists on dynamic communications between different brain regions.

This work describes our efforts at creating a reliable research tool for neuroscientists to safely explore the opportunities provided by LIFUP technology to study the brain and neuronal activity. Prior studies into effective treatment regimens have indicated a need for pulsed waveforms, at pulse repetition frequencies (PRFs) between 10 and 1000 Hz, and duty factors from 5% to 50%. We have specifically developed a device suitable for use in an MRI, with single-focus transducers coupled to an electronic drive system that automatically sets the nominal ultrasound exposure parameters, thus simplifying the experimental process for the user.

II. System Development

The goal is the stimulation or suppression of areas of the brain using controlled ultrasound pulse sequences from a focused transducer capable of operation in an MRI environment. The device used for the initial LIFUP experiments [17], [23], [24] comprised individual electronic components (i.e., waveform generator, power amplifier, and power meter) assembled on a rack mount and controlled from a standard Windows computer. While satisfactory for early laboratory work, the system was difficult to transport, and its operation was limited to expert users. Therefore, a design effort was conducted to reduce its size, increase its usability, and improve its operational safety.

At the same time, the transducer, transducer holder, and positioning features were revised to provide a more convenient and consistent approach to applying the transducer to the participant's head and determining its position relative to brain structures of interest.

As described further below, the key features of the system (BX1002) are flexibility in treatment parameter selection, the exacting calibration of the electronics and transducers, the self-monitoring of the system to prevent both undertreatment and overtreatment, and the simplified approach to accurately target the transducer through angulation and position imaging. In comparison with the original device, the new system is smaller (80% reduction), lighter (85% reduction), and fully integrated (a single case and a monitor), allowing portability and tabletop operation.

A. System Description

The revised system consists of three parts: 1) the Stimulator, programmable to administer a variety of voltage and pulse sequences to the transducer; 2) single-element focused ultrasound transducers suitable for use in the MRI (MR conditional [25]); and 3) an MRI safe transducer holder that can be positioned and attached to the participant/patient's head to hold the transducer in a specific position while still fitting within an MRI head coil. Fig. 1 provides a schematic illustration of the system.

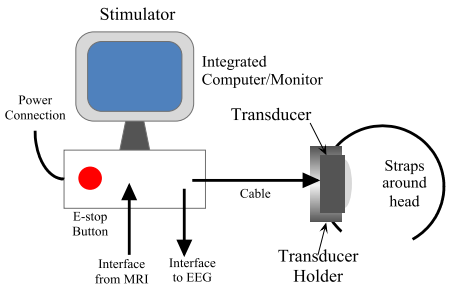

Fig. 1. Overall System components.

The Stimulator, shown in Fig. 2, has a dedicated all-in-one computer (POC-155, Advantech) and an ultrasonic drive generator. The ultrasonic drive voltage is provided through a BNC panel mount connector on the front panel. The ultrasonic drive circuitry produces a bipolar, pulsed quasi-sinusoidal (shaped square) waveform with controllable voltage amplitude, ultrasonic drive (carrier) frequency, pulse duration/width, and PRF. It also includes supervisory circuits and signal isolation (see Fig. 3).

The core of the generator is a complex programmable logic device (CPLD XC2C384, Xilinx) running at 50 MHz. It is interfaced to the Advantech computer via USB 2.0. This CPLD provides the control, timing, and interface functions for the subcircuits described below.

A programmable voltage power supply may be set from a minimum output of 1.5 volts to a maximum output of 50 volts. Since the system is generally set to maintain a standard average power over a wide range of pulse duty factors, the power supply has a low-voltage (1.5–15 V), high-current (1 A_{rms}) section, and a higher voltage (15–50 V), low-current (0.2 A_{rms}) section. The circuit topology of the two sections are essentially identical, based around a switching regulator (LT1738, Linear Technologies) in a flyback configuration and external N-channel enhancement mode MOSFET (Diodes Inc.). The two sections use different winding ratios (1:1 or 1:3) in the flyback transformer (VERSA-PAC, Eaton Electronics), and other specific component values are selected to match the voltage and current ranges. A 16-bit D/A converter (DAC8552, Analog Devices) sets the voltage applied to the feedback inputs of the regulators and allows the voltages to be digitally controlled. A relay switches between the two power supply sections depending upon the desired output. The supply supports a peak transmitter output of 120 W while transmitting and an average power output of 6.0 W.

The output of the power supply is fed to the input center tap of a coupling transformer, and the other two transformer connections are connected to ground via N-channel MOSFETs (FDT86244, Fairchild). By alternately enabling each MOSFET (TC4426, Microchip), the transformer input reverses polarity, producing the bipolar output swing. A slight delay is

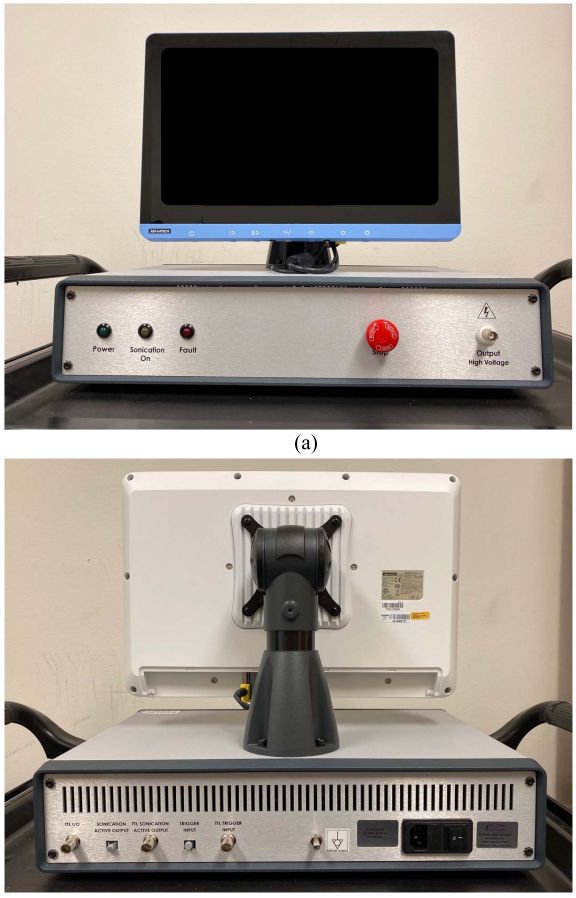

(a)

(b)

Fig. 2. (a) Stimulator—Front. From left to right, the indicator lights include power, sonication ON, and fault. Large button is emergency shutdown. Connector on the right is for the transducer cable. (b) Stimulator—Rear. From left to right, connectors include TTL I/O, sonication active output (optical connection), TTL sonication active output, trigger input (optical connection), and TTL trigger input. The master grounding pin is in the center. Connector on the right is the power input module.

introduced into the drive timing to ensure that both MOSFETs are not active at the same time. This produces a bipolar pulse of approximately twice the transmitter power supply voltage (2.5–62.5 V_{rms} into a 24-Ω resistive load). The output can be switched via a relay either to an output isolation transformer or to 100-Ω/2-W resistors which are used during the voltage calibration process. The output stage also includes resistors that provide 50-Ω output impedance; they also provide a load resistance in case the system is operated without a transducer connected.

The operator does not set the drive voltage directly but instead specifies the desired ultrasound exposure parameters (pressure, average intensity, pulse length and PRF, sonication duration, intersonication time, and number of sonications), and the system calculates the voltage required to meet these settings using transducer calibration information. Note that the pressure and intensity values are based on the hydrophone data taken in water: the system does not attempt to estimate actual *in situ* values (see Section IV). If the system cannot attain the desired output settings because of hardware voltage or power limitations or the overall safety limits imposed on the system, then the operator is notified.

The ultrasonic drive frequency of the device is adjustable from 250 kHz to 1.25 MHz, in frequency increments of 50 kHz, using a direct digital synthesis chip (AD9834, Analog Devices). Note that the current transducers are designed to operate only at 650 kHz. Using the CPLD logic functions, both the pulse length and PRF are derived from the ultrasonic drive frequency and constrained to be an integer number of cycles, thus providing synchronous control and avoiding "runt" pulses. The PRF is adjustable over the range from 3 Hz to 1.5 kHz, and the pulse length is adjustable in increments of 20 μs. The PRF resolution is as follows: for PRF values below 100 Hz, the resolution is better than 0.2 Hz, for PRF values up to 725 Hz, the resolution is better than 10 Hz, and for PRF values up to 1000 Hz, the resolution is better than 20 Hz. The maximum pulse length is greater than 1 s. The system is capable of producing pulse sequences of selectable total exposure duration up to several minutes in length.

The drive level is monitored to provide protection against improper outputs using both software methods and a fail-safe "hardware only" protection circuit. Both the maximum and average voltages are monitored by the safety circuits and the output is shut down if predefined limits are exceeded.

The maximum voltage is derived from the transmit power supplies (before the center-tap transformer) using a 20:1 resistive voltage divider. The average pulse drive voltage is sensed after the transformer stage through a 25:1 resistive voltage divider. Because this signal is bipolar and the average voltage is zero, it is first rectified and then filtered through an active four-pole Bessel filter (an F_{cutoff} of 15 Hz and a step resolution of less than 0.3 s). This approach was found to provide a stable value over a range of transmit conditions.

For software monitoring, the transmitter power supply voltage and the pulse drive voltage are A/D converted (LTC1865, Analog Devices) and continually available to the software. In addition, analog comparators check the two voltages against trip levels for each; the trip voltages are set with digitally programmable voltage sources using nonvolatile storage. A hardware fault will halt treatment and illuminate a front panel fault indicator. This provides both software and hardware protection against excessive outputs, while software can also provide verification that the output drive level is appropriate, i.e., at the specified level. If the drive does not match the set level, the software disables the transmit function and notifies the operator.

As an additional safety feature, the transmitter electronics provides a "timeout" timer that must be read and reset by the system computer via a USB command every 1 s. If the system software does not provide a reset within the timeout period, the transmitter hardware disables the transmit electronics and disconnects the transmitter from the output connector and illuminates the front panel fault indicator. In addition, if the software does not read an active "timeout" bit every second, it assumes that the hardware has malfunctioned and must be disabled. A two-port USB interface is provided where one port is used for all normal operations, while the other port is used to provide the "timeout" interface and shutoff capability to the PC.

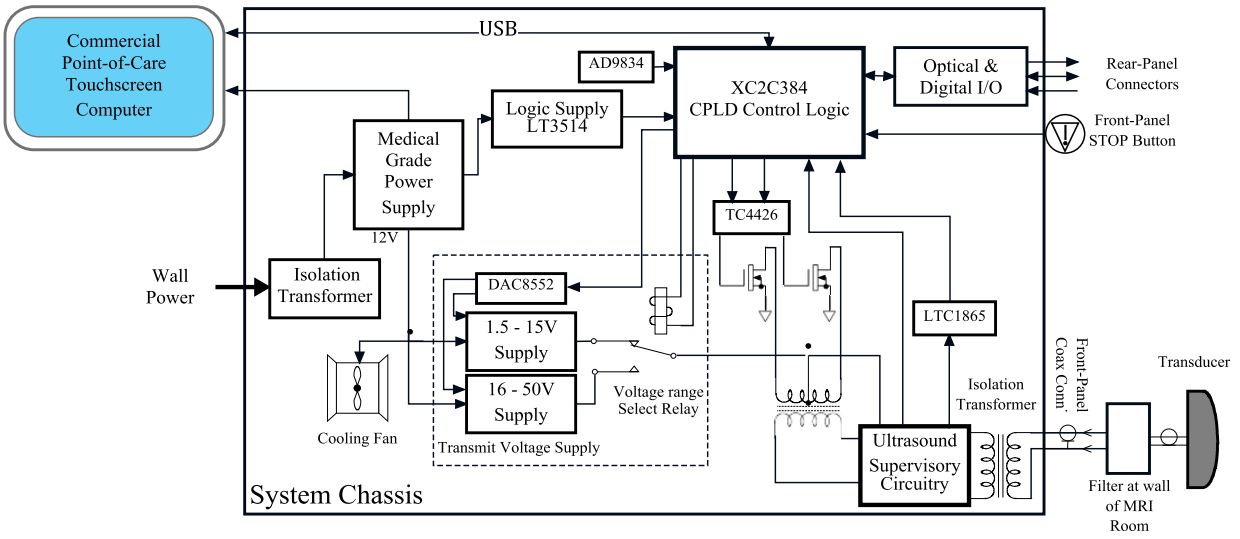

Fig. 3. Stimulator internal configuration.

MRI synchronization is provided via a fiber optic input line and an optically isolated digital signal line (TTL signaling). This allows for the ultrasound to be turned on synchronously with MRI, allowing for simultaneous collection of blood oxygenation dependent imaging (BOLD) data. EEG synchronization is also provided, in which the system outputs a signal to the EEG during the time of ultrasound transmission [again either TTL or optical, see Fig. 2(b)]. This allows for synchronization of the recording of ultrasound stimulation with the EEG recordings.

B. Transducer, Transducer Holder, and Transducer Alignment Markers

The system uses circular, single-element, spherically focused transducers (Blatek, State College, PA), with an active aperture of 61 mm. Three different transducers were designed, with nominal focal lengths of 55, 65, and 80 mm, as required for targeting different regions of the brain [see Fig. 4(a)]. The transducers use 1–3 piezocomposite material with a low loss backing to provide an average bandwidth of 21% (which is appropriate for a low-power, nonimaging design). The design includes a slightly convex front layer for impedance matching. The convexity makes it easier to remove any air bubbles when applying coupling gel pads. The measured focal peak pressure locations are typically found 1–2 mm shallower than the nominal transducer radius of curvature (as expected). Table I summarizes their beam characteristics, as measured in water.

Early tests were also conducted with 71-mm aperture diameter transducers, but it was found that the larger size was difficult to position on the skull because it overlapped the patient's ear and was harder to maneuver inside an MRI head coil, so the final design was limited to 61 mm.

Because the transducers contain electrically conductive materials, i.e., wires and conductive plating, they cannot be classified as MR safe. Instead, the transducers are designated MR conditional [25] and have been deemed to be safe in a 3-T MRI environment, having been tested for torque and interference. There was no interaction at 128 MHz with the scanner RF transmit and receive coils, but this interaction may be frequency dependent. This is because the Larmor frequency of an ^{1}H atom is dependent on the magnetic flux density (42.57 MHz/T). As such, there may be possible interference at other MR field strengths. The transducer plastic housing (machined polyoxymethylene, Dupont Delrin) contains the 650-kHz piezo-element and enables the transducer to be affixed within the transducer holder, which is held in place using an adjustable strap. The transducer has a 5 m long MR conditional cable, which connects to the Stimulator console through a wall filter (Mini-Circuits BLP-15+) and an additional 5 m of cabling (see Fig. 3). This allows the Stimulator console to be located outside of the MRI suite. Each transducer is individually calibrated as described in Section III.

TABLE I
TRANSDUCER BEAM CHARACTERISTICS

In-Water Data (mm)	Transducer Nominal Focus		
	55mm	65mm	80mm
Focal Peak Depth	54	63.5	78
Near -6dB Depth	43.6	50.4	60
Far -6dB Depth	68.4	80.5	102.5
-6dB Focal Width	3.8	4.0	4.4

It is essential that the transducer be positioned comfortably yet securely against the temporal region of the scalp. Further, the transducer and holder arrangement must fit inside the MRI head coil. A low-profile, MR safe (3-D printed from urethane methacrylate) transducer holder was developed (Archimedic Inc, Newtown Square, PA) that allowed for simple positioning and angulation [see Fig. 4(b) and (c)].

The holder has a series of internal grooves, and the back of the transducer has been designed with an integral, spring-tensioned clip mechanism that matches the grooves [see Fig. 4(a) and (b)]. The clip mechanism is virtually identical to that used in snap-on, center pinch camera lens covers,

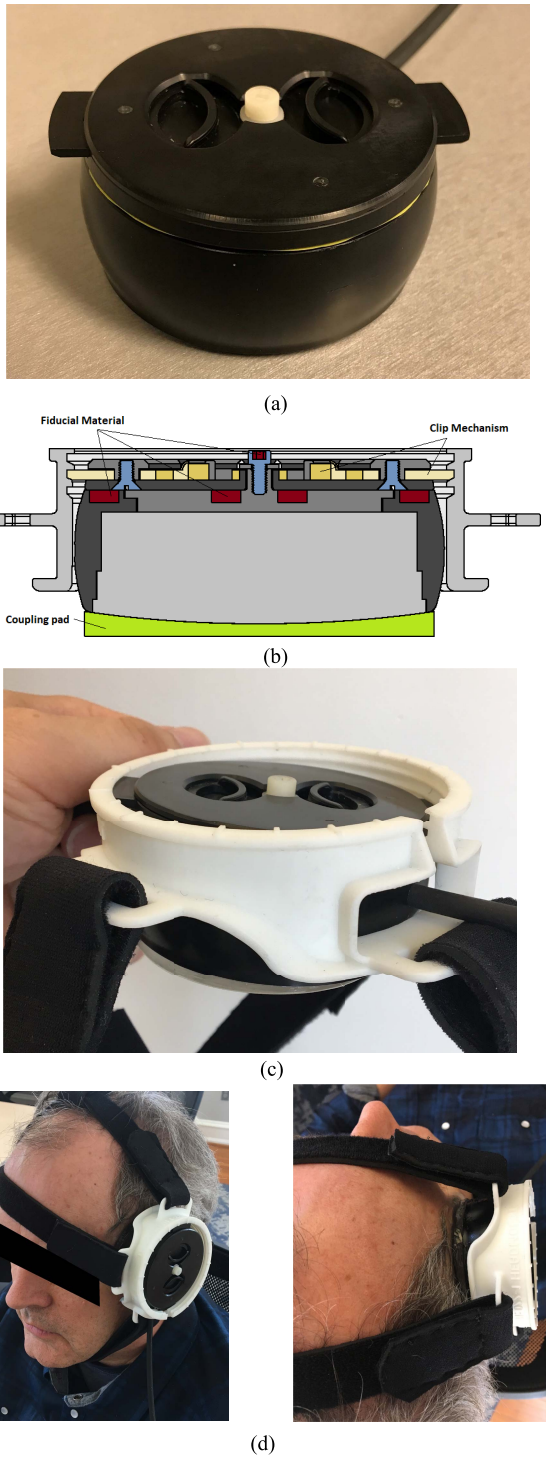

Fig. 4. (a) Transducer showing the clip mechanism. (b) Simplified cross section of the transducer and holder showing the clip mechanism (tan), fiducial materials (red), and coupling pad (green). (c) Transducer and transducer holder showing the clip mechanism in grooves to set angular position. (d) Transducer and transducer holder on subject's head, front and top views.

with the internal spring comprising machined Delrin material. By aligning the clip and grooves, the transducer can be positioned at 0°, 2.5°, or 5° from normal with respect to the skull surface [see Fig. 4(c)]. By rotating the clip mechanism within the outer housing, the direction of angulation can be changed (precessed) over a full 360°. The positioning of the transducer on the skull is shown in Fig. 4(d).

Fig. 5. Coupling pad with imbedded rim, mated to the transducer. Note that the air bubbles seen between the gel pad and transducer face would be removed before use.

Customized acoustic gel pads (based on Aquaflex, Parker Labs) have been designed to fit the transducer and are intended to be used as coupling media, along with standard acoustic scanning gel. Each gel pad is preformed to a specific angle of 0°, 2.5°, or 5°, in order to maintain good acoustic coupling as the transducer is angulated. The gel pads have an embedded plastic rim (FDM-printed Ultem 9085) to lock them in place against the transducer face (see Fig. 5).

The transducers have a unique feature to assist with the alignment process. Two rings of highly MRI-visible material [26] are built into the back of the transducer (Styrene block polymer). Additional material is placed in the center of the screw that holds the back of the transducer [see Fig. 4(b)]. These fiducial markers allow the exact spatial orientation of the transducer to be determined. Examples of MRI images of the transducer and markers are shown in Fig. 6(a) and (b). The images were not acquired perfectly perpendicular to the fiducial rings but were rotated after acquisition to facilitate targeting. Fig. 6(a) shows the transducer in relationship to the participant's ear. Fig. 6(b) illustrates the alignment process. The center of the concentric rings locates the axis of the ultrasound beam (top left image). The red line in the top right and bottom images delineates the plane of the rings and transducer. A line drawn perpendicular to the plane of the rings through the center screw (blue and green lines in the top right and bottom images) established the central acoustic axis. The position of acoustic focus within the brain can be estimated using the measured transducer focal depth (as described in Section III) placed along the line of the acoustic axis determined using the fiducial markers. The gel pads used for acoustic coupling also are highly visible within the MRI image, making it easier to determine the exact position of the transducer and skull surfaces. Fig. 6(b) corresponds to Fig. 4(d) in terms of spatial orientation.

Fig. 6(c) shows an overlay of the Fig. 6(b) image, with an oval that represents the focal location based on hydrophone measurements taken in water. While the actual focal zone *in situ* is beyond the capabilities of the system to predict for the specific patient being treated, the display of the in-water

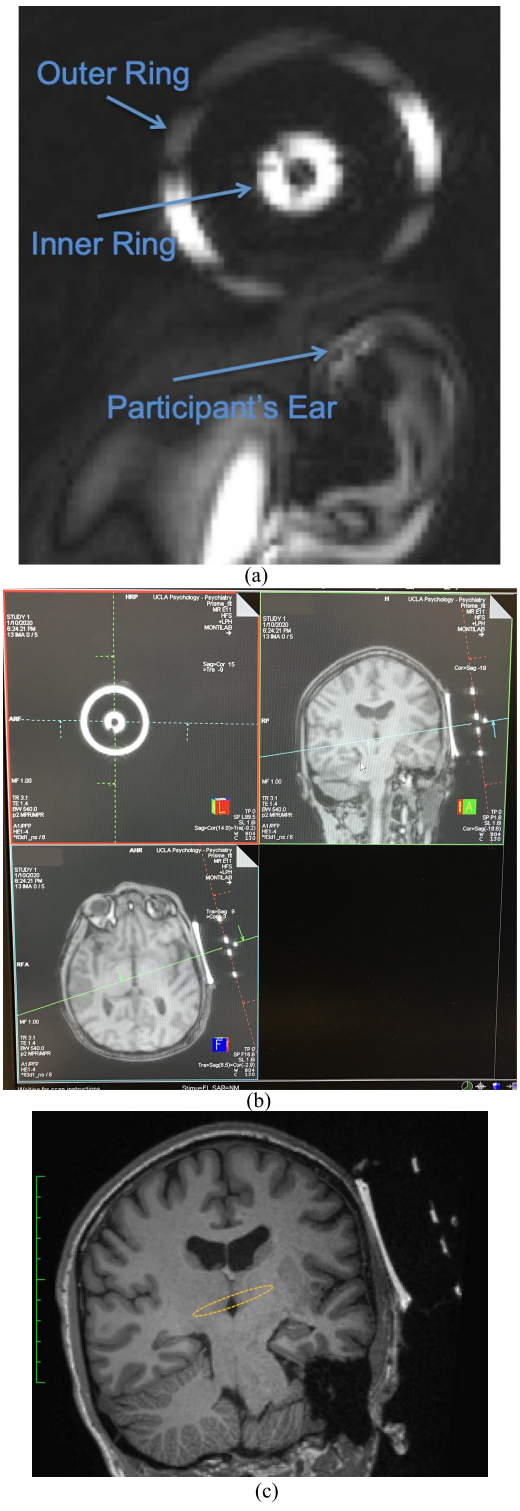

Fig. 6. (a) MRI image of transducer fiducial markers. (b) MRI image of the transducer on subject's head, showing the alignment process using the fiducial markers. (c) MRI targeting image of the transducer on subject's head, showing the approximate position of the focal zone based on the fiducial markers. The oval represents the approximate position of the −6-dB focal region, as measured in water, for an 80-mm focal depth transducer.

focal characteristics gives the operator a general sense of the volume to be insonified, for the purposes of the initial transducer alignment. The final transducer positioning guidance for treatment uses fMRI techniques (see Section V).

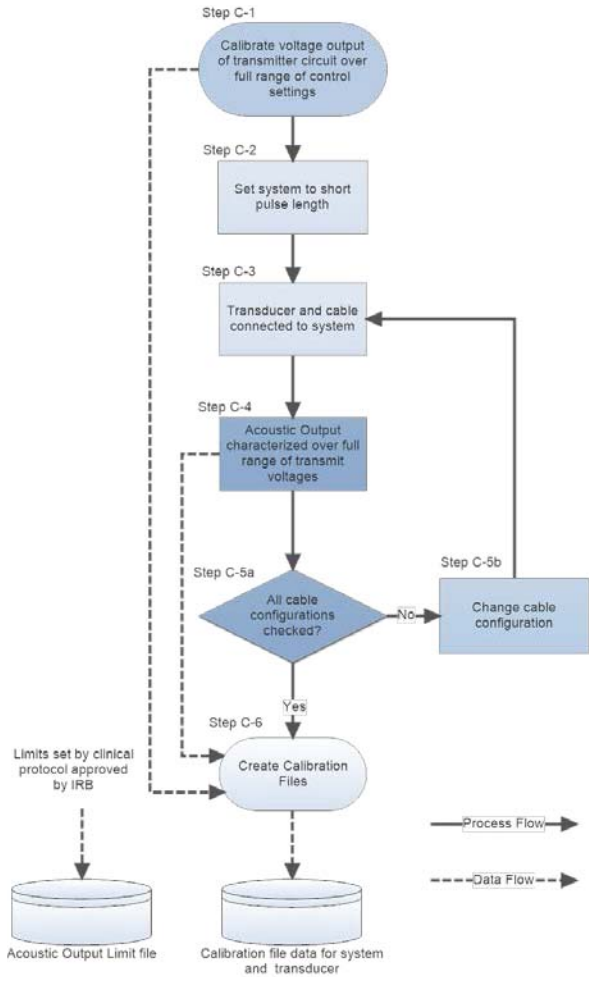

Fig. 7. Calibration process.

III. Calibration Techniques

The purpose of the calibration process is to assure that the desired ultrasound exposure is provided on a repeatable consistent basis. The steps are outlined in the two flowcharts (Figs. 7 and 8). This process is conducted for every Stimulator, in combination with any specific transducers that are supplied with the system.

Because of slight tolerance variations in the components used in the transmitter electronics, the first step is to calibrate the digital control of the electrical transmit voltage. During calibration Step C-1, the transmit voltage is measured over the full range of digital control settings. This information is then made available as a calibration file stored on the system in Step C-6. The system is set to a nominal short pulse length transmit condition (Step C-2). Once a calibrated relationship has been established for a specific pulse duration or length, the average intensity can be derived for any other pulse duration and PRF. This obviates the need to measure all possible transmit conditions. In Step C-3, a specific transducer and cable are connected to the system. The serial number of the transducer and the specific cable configuration are recorded so that they are included in the calibration file data.

In Step C4, a calibrated hydrophone is used to measure the acoustic output from the transducer/cable combination.

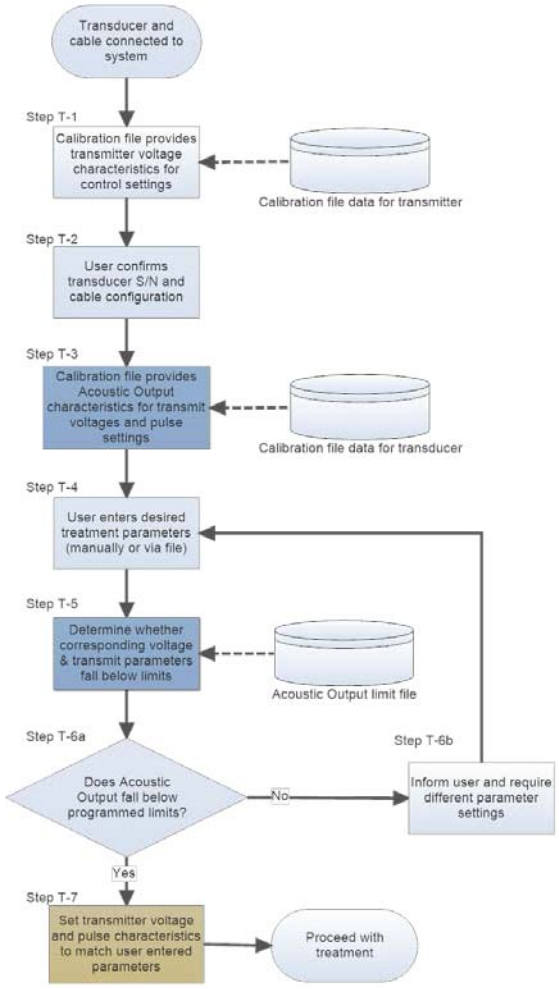

Fig. 8. Treatment setting process.

The measurement process includes finding the spatial location of the maximum acoustic output, characterizing the pressure and intensity at that location, and also scanning around that location to find the −6 dB extent of the ultrasound beam [27]. Transducer variability tolerances have been set at 5% of the nominal focal depth, 5% relative to the average focal width (see Table I), and 10% relative to the average transducer efficiency (pressure/voltage ratio, see below). Transducers outside these ranges are rejected or reworked.

At output drive levels from 1.5 to 16 V, polyvinylidene difluoride (PVDF) bilaminar membrane hydrophones [28] are used for primary measurements of focal zone characteristics and voltage/pressure relationships, and for cross-checking the results. The hydrophones are calibrated and maintained to international standards [29], [30]. However, as the transmit voltage is increased, cavitation can cause both interference with the measurements and damage to the hydrophone. A scattering hydrophone [31] is therefore placed at the focal location, and measurements are taken for output drive voltages between 4 V (lower sensitivity limit of the hydrophone) and 50 V (system maximum). Since the scattering hydrophone is not independently calibrated, its results are compared with the bilaminar hydrophone results over the range where data are available from both (4–16 V) to develop a hydrophone cross-calibration factor [28]. The measurement results show that the cross-calibration factor is consistent over this voltage range (coefficient of variance of less than 1%). The scattering hydrophone data are then used for higher transmit voltages.

At the maximum output drive voltage of 50 V, the typical focal pressures (maximum $p_{r.0}$) range from 2.6 to 3.8 MPa depending upon the focal length of the transducer (at the minimum drive voltages, the pressures range from 85 to 125 kPa). The measured $p_{r.0}$ is very linear with drive voltage (e.g., $p_{r.0} = 0.064$ MPa/V, R^2 of 0.9961). If the system was operated in continuous wave mode (which it cannot do), those maximum pressure levels would correspond to spatial peak intensities ($I_{SPTA.0}$) of ∼300–500 W/cm^2. The calibration process is repeated using any other cables and RF filters that may be expected to be used in the clinical environment. This is documented in Steps C-5a and C-5b, which loop back to Step C-3 until all transducer/cable combinations have been tested. Investigators were reporting that they wanted to position the patient further from the stimulator and were adding "extension" cables to the transducer. Further, they wanted to use the isolation panels to connect the transducer inside the MRI to the console in the control room, rather than running the cables through holes in the panels. Having additional cable between the drive circuits and the transducers produces additional capacitive load and electrical loss and introduces the possibility of transmission line phenomena. Using the filters provided in the isolation panels also reduced the signal available to the transducer. Experiments with different configurations showed up to a 40% loss in peak pressure at the transducer focus, relative to a "direct" (5 m cable only) connection between the transducer and stimulator. Therefore, the outputs of the transducer are calibrated with longer (10 m) cables and specified filters, so that the treatment conditions could be the same irrespective of the particular setup (short cables or long cables with filters). Because each treatment requires the use of a corresponding calibration file (which lists the transducer serial number and the cable configuration), the output from the transducer to the patient is maintained within the treatment parameters.

Although not shown in the diagram, the process from Steps C-2 to C-6 is repeated for additional transducers as necessary. As the final step, calibration files are generated (Step C-6), which contain information specific to the Stimulator, transducer, and all related cable/isolator connections. In addition, a file is created which establishes the limits on the acoustic output/treatment conditions. These limit files are matched to the specific clinical study being conducted at the facility that houses the system.

When using the system, the operator has a specific transducer and cable configuration, the serial number of which is already entered into the system as default conditions, based on the prior treatment. The first step is to retrieve the transmit voltage calibration data (Step T-1). Next, the user confirms the transducer serial number and cable configuration (Step T-2). With that information, the system retrieves the acoustic output characteristics from the calibration file data (Step T-3).

The user/operator enters the desired treatment parameters using a treatment parameter file and front panel controls

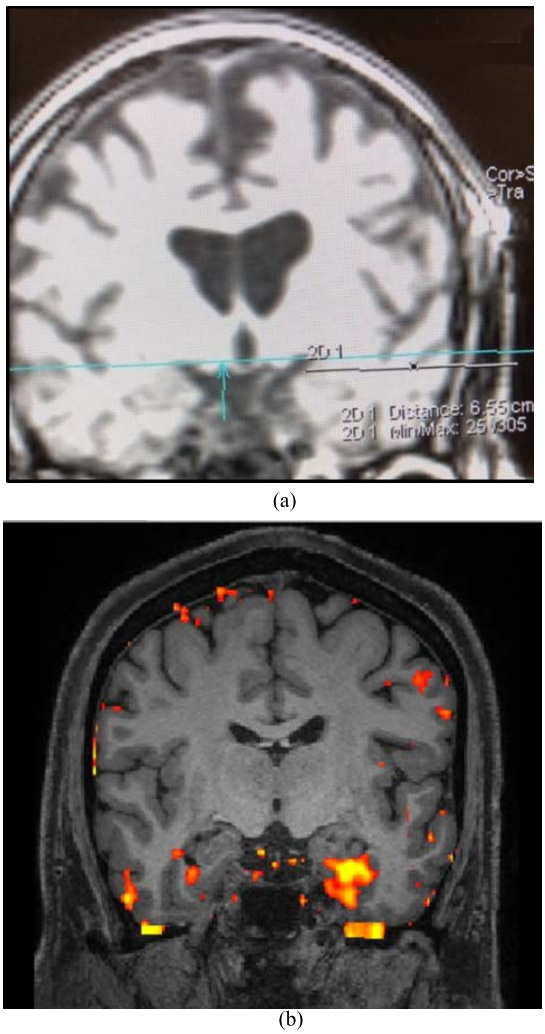

(a)

(b)

Fig. 9. Example of pre- versus post-LIFUP focal perfusion changes (see text for details). (a) Targeting image with the expected acoustic axis, using the methods described earlier [see Fig. 6(b) and (c)], prior to stimulation. The blue line denotes the acoustic axis, and the separate black line shows the depth to the focal region (65 mm). (b) Resultant increase in bloodflow in the entorhinal cortex due to stimulation. Warmer colors are indicative of a greater increase.

(Step T-4). Based on the acoustic output limits established for the clinical study protocol by the Institutional Review Board (IRB), the system determines whether the entered treatment parameters exceed the limits, as shown in Steps T-5 and T-6a. If the limits are exceeded, the user is informed and required to set different parameters which are in compliance with the limits (Step T-6b). Once the parameters selected by the user comply with the acoustic output limits (looping through Steps T-4 and T-6), the transmitter voltage and pulse characteristics are set to match the user entered parameters (Step T-7) and the system proceeds to treatment.

IV. Output Limits and *In Vivo* Exposure Values

A. Output Limit Considerations

A key goal of LIFUP treatment is to induce the neuromodulatory effects without causing any damage to brain tissue. This is in contrast to high-intensity focused ultrasound (HIFU), which is specifically designed to cause tissue ablation or other effects, either through thermal or nonthermal means. Further, LIFUP study participants are often healthy volunteers, for instance, in investigations of brain mapping, or perception or motor effects [7]–[9], [32]. Therefore, the risk/benefit assessment for such studies must prioritize the safety of the ultrasound exposure.

There are no established regulations or guidelines for therapeutic ultrasound exposure limits, thus complicating the process of determining what a "safe" exposure might be [33]. The issue is further confounded by the patient-to-patient variability of the skull, which reflects, absorbs, and refracts the ultrasound beam, reducing the pressure levels and distorting the focal region.

Given these uncertainties, it was felt that an appropriate approach would be to use the intensity and pressure-based limit guidelines established by the US Food and Drug Administration (FDA) for diagnostic ultrasound equipment [34]. While the FDA maximum values were not originally based on safety considerations, diagnostic ultrasound has had an outstanding record of patient safety in the 30 years since the FDA Guidance was first promulgated.

The FDA has set a maximum focal spatial-peak, temporal average intensity of 720 mW/cm^2 (nonophthalmic applications), assuming a uniform tissue attenuation or derating of 0.3 dB/cm·MHz (denoted $I_{SPTA.3}$) [34]. At an operating frequency of 650 kHz and a focal distance of 75 mm, that limit corresponds to a nonderated $I_{SPTA.0}$ of approximately 1 W/cm^2, which is the value noted by the American Institute of Ultrasound in Medicine (AIUM) for not producing thermal bioeffects with focused ultrasound fields [35].

Similarly, the peak rarefactional pressure (p_r) is set by a limit on the mechanical index (MI), which is the derated p_r divided by the square root of frequency in megahertz. The FDA MI limit is 1.9, which for the frequency and focal conditions noted above correspond to a nonderated $p_{r.0}$ of 2.3 MPa. This is well below the theoretical threshold for bubble nucleation and subsequent inertial cavitation [36]. It should be noted that the MI was derived for the case of short bursts of ultrasound (a single cycle) and is not entirely applicable to longer pulse lengths. Nonetheless, MI has become a common metric in describing all types of ultrasound exposures.

While the FDA derating approach for diagnostic systems is not completely predictive of the therapeutic transcranial situation, it does provide an upper bound on *in situ* exposure. Abiding by the diagnostic ultrasound limits ensures that the LIFUP treatment exposure is comparable to or lower than diagnostic procedures such as TCD. This approach, at least for the initial studies of this new treatment modality, has provided a level of safety assurance that eased the IRB approval process and allowed many clinical investigations to be deemed "nonsignificant risk" (NSR).

B. Estimation of In Vivo Exposure

Based on these safety and regulatory considerations, the Stimulator displays both the derated and nonderated I_{SPTA} and rarefactional pressure values. However, the actual

pressures and intensities in the brain are a function of the thickness and nonuniformity of the patient's skull and are beyond the capabilities of the system to predict. It is, therefore, left to the operator to estimate based on any of a number of methods [21], [37]–[40].

As a check on the possible distortion of the ultrasound beam, we conducted *in vitro* measurements of transmission through cadaveric temporal bones ($N = 5$). The beam characteristics of a 65-mm nominal focus transducer were compared with and without temporal bone samples placed in the acoustic path. This transducer was chosen as representative of the three focal lengths. On average, the broadening of the −6-dB lateral focal width was 1.5 mm, the lengthening of the −6-dB axial focal length was 1.4 mm, and the lateral shift was less than 1 mm (compare to in-water data from Table I). Thus, the representation of the focal zone shown in Fig. 6(c) is sufficient for the purpose of the initial transducer alignment. The measured focal pressure reduction caused by transmission through the temporal bones was 15.9 ± 4 dB, which is comparable to other reports in the literature [21], [40]. Thus, it is clear that the *in situ* pressures and intensities are far below the comparable regulatory limits, further ensuring the safety of the treatment.

In a separate investigation, exposures up to eight times the intensity limit (up to $I_{SPTA.3}$ of 5760 mW/cm^2) failed to produce a measurable *in situ* temperature rise via MR thermometry [41].

Because the system is designed to not produce significant thermal changes in the brain, it is not possible to use MR thermometry as a targeting approach. Therefore, fMRI has become the principal means of checking the position of the focal region *in situ*. This is discussed in Section V.

V. Examples of fMRI Changes

Fig. 9 shows an example of localized stimulation of brain tissue using LIFUP. This is a representative sample image from a single participant recruited under an IRB-approved study conducted at UCLA (IRB: 18-000104). Fig. 9(a) shows the targeting process, with the center of the acoustic axis shown in blue [compare to Fig. 6(b)]. A separate line (in black) is superimposed to show the approximate location of the focal region for the transducer used in this study (65 mm). Fig. 9(b) shows LIFUP-induced changes in cerebral blood flow as measured using pulsed Arterial Spin Labeling (ASL) (1.5 × 1.5 × 3 mm voxels, TR = 4600 ms, TE = 16.18 ms, TI = 1990 ms, BD = 700 ms, FAIR QII perfusion, 3-D turbo GRASE sequence, turbo factor = 20) collected using a Siemens 3T Prisma scanner. The ASL images are acquired before and after LIFUP stimulation. The resultant sequences are processed using FSL v 6.0.1 (FMRIB Software Library, Oxford, U.K.) and then subtracted to create a difference image to illustrate changes from baseline to post-LIFUP. This image is then overlaid on a high-resolution structural T1-weighted image in order to generate the image shown in Fig. 9(b). We emphasize that this is an individual participant and not a group average, and while the LIFUP neuroimaging results have been consistent across participants, not enough participants have been studied to determine the sources of this variance. This work is preliminary and ongoing.

The transducer used in this study has a 65-mm focal depth, with a 61-mm diameter. The ultrasound transmit parameters were 942 mW/cm^2 $I_{SPTA.0}$ (720 mW/cm^2 $I_{SPTA.3}$), 100-Hz PRF, 5% duty cycle, 0.71 MPa $p_{r.0,}$ and 30 s ON/30 s OFF for one 10-min treatment block. The resultant change in the entorhinal cortex is in the focal region. The activations near the focus are presumed to be a direct effect of the LIFUP, while the other activations are presumed to be indirect effects via the functional connectivity of the focal region. Note that some of the apparent activations in this particular slice are not in the brain itself. While the possibility that some apparent activations may simply be noise cannot be ruled out, this approach nonetheless offers the potential for the interconnections between brain regions to be examined and mapped.

A. Selected Recent Clinical Results

Over the past few years, this technology has been used for a variety of clinical applications. As rigorous trials have not yet been completed in clinical populations, these results are far from conclusive. We present here a few preliminary but promising observations.

In 2015, a case series was presented demonstrating the preliminary safety and feasibility of using focused ultrasound to modulate the activity of the brain in the epileptogenic focus [23]. This study, conducted under an investigational device exemption (IDE) issued to BrainSonix, explored noninvasive brain stimulation with focused ultrasound with derated spatial-peak temporal-average intensities of up to 720 mW/cm^2.

In the initial safety study on epilepsy patients, participants received the ultrasound stimulation prior to scheduled surgical resection of the diseased epileptic brain tissue. Using standard histology measures (i.e., hematoxylin and eosin staining), investigators looked for histological changes to the tissue caused by the ultrasound and were not able to find any changes due to the ultrasound.

In the interest of further establishing safety criteria, similar parameters were used in *ex vivo* experiments at much higher intensities to attempt to determine where is the safety threshold for *in vivo* stimulation [42]. Using the average cell volume as a proxy for damage, samples of tissue that were sonicated at intensities up to 12 000 mW/cm^2 were compared to samples of tissue from the same participant that did not receive any sonication at all. Samples were all postmortem cases with tissue taken within 24 h after the time from death. Between six to eight samples were obtained from the temporal lobe of each of the participants. After correcting for multiple comparisons, none of the cells at each intensity level were statistically significantly different from the control cells. Furthermore, a board-certified neuropathologist who was kept blinded to the intensity levels was not able to distinguish between slides from sonicated brain tissue and unsonicated brain tissue. This study showed that focused ultrasound at the aforementioned

intensities did not produce changes that could be detected either by board-certified neuropathologists or by computer analytic programs [43].

In 2016, the technology was first utilized in man for noninvasive deep brain stimulation of a patient with a disorder of consciousness [24]. This patient had suffered a traumatic brain injury resulting from a car accident. After standard neurocritical care procedures failed to arouse the patient from a minimally conscious state, the patient underwent 5 min of focused ultrasound treatment spread over 10 min (e.g., 30 s ON, 30 s OFF). The ultrasound transmit parameters were 960 mW/cm^{2}I$_{SPTA.0}$ (720 mW/cm^{2}I$_{SPTA.3}$), 100-Hz PRF, 5% duty cycle, and 0.7 MPa $p_{r.0}$, all of which were adapted from [44]. Three days after LIFUP, the patient had made dramatic improvements, demonstrating full language comprehension and reliable response to commands. After five days, the patient attempted to walk. We should note that while the improvement was impressive, a spontaneous and serendipitous recovery cannot be ruled out. Further studies of patients in minimally conscious states are ongoing.

VI. Future Goals and Opportunities

The goal of this work was to provide a well-calibrated, simple-to-use ultrasound stimulation system for neuromodulation studies. It provides a single-element transducer design and a straightforward control mechanism, with extensive calibration and internal electronic monitoring to prevent unwanted over or under treatment. This approach relieves researchers of many of the details associated with developing their own exposure equipment. The unique MRI fiducial targets and transducer positioning system simplify alignment and targeting. While the system does not provide positional precision afforded by devices intended for ultrasonic surgery (i.e., HIFU), the intended goal of transient neurostimulation does not require the same precision as permanent tissue ablation [45].

The future applications for the technology could potentially include not only treatment of epileptic episodes and amelioration of disorders of consciousness but also neuropsychiatric conditions such as depression, anxiety, pain, obsessive/compulsive disorder (OCD), and delivery of exosomes and small molecules. The safety profile allows the technology to be applied more broadly to a wider range of patients and also allows for repeat exposures for the treatment of chronic conditions.

Acknowledgment

The authors would like to thank Dr. Taylor Kuhn (Department of Psychiatry and Biobehavioral Sciences, UCLA) and Dr. Martin Monti (Department of Psychology, Department of Neurosurgery, UCLA) for providing some of the images used in this article. Dr. Nicolas Ellens (Acertara Acoustics Laboratories) worked with the authors to obtain the skull attenuation data and James Gessert (Acertara Acoustics Laboratories) provided significant electronic design assistance.

References

[1] W. J. Fry, "Intense ultrasound in investigations of the central nervous system," *Adv. Biol. Med. Phys.*, vol. 6, pp. 281–348, Jan. 1958.

[2] A. Bystritsky *et al.*, "A review of low-intensity focused ultrasound pulsation," *Brain Stimul.*, vol. 4, no. 3, pp. 36–125, Jul. 2011.

[3] A. Bystritsky and A. S. Korb, "A review of low-intensity transcranial focused ultrasound for clinical applications," *Current Behav. Neurosci. Rep.*, vol. 2, no. 2, pp. 60–66, Jun. 2015.

[4] K. R. Foster and M. L. Wiederhold, "Auditory responses in cats produced by pulsed ultrasound," *J. Acoust. Soc. Amer.*, vol. 63, no. 4, pp. 1199–1205, Apr. 1978.

[5] K. Hynynen, N. I. Vykhodtseva, A. H. Chung, V. Sorrentino, V. Colucci, and F. A. Jolesz, "Thermal effects of focused ultrasound on the brain: Determination with MR imaging," *Radiology*, vol. 204, no. 1, pp. 247–253, Jul. 1997.

[6] W. J. Tyler, Y. Tufail, M. Finsterwald, M. L. Tauchmann, E. J. Olson, and C. Majestic, "Remote excitation of neuronal circuits using low-intensity, low-frequency ultrasound," *PLoS ONE*, vol. 3, no. 10, Oct. 2008, Art. no. e3511.

[7] Y. Tufail *et al.*, "Transcranial pulsed ultrasound stimulates intact brain circuits," *Neuron*, vol. 66, no. 5, pp. 681–694, Jun. 2010.

[8] W. Lee, H. Kim, Y. Jung, I.-U. Song, Y. A. Chung, and S.-S. Yoo, "Image-guided transcranial focused ultrasound stimulates human primary somatosensory cortex," *Sci. Rep.*, vol. 5, no. 1, p. 8743, Mar. 2015.

[9] W. Legon *et al.*, "Transcranial focused ultrasound modulates the activity of primary somatosensory cortex in humans," *Nat Neurosci.*, vol. 17, no. 2, pp. 322–329, Feb. 2014.

[10] J. Mueller, W. Legon, A. Opitz, T. F. Sato, and W. J. Tyler, "Transcranial focused ultrasound modulates intrinsic and evoked EEG dynamics," *Brain Stimul.*, vol. 7, no. 6, pp. 900–908, Dec. 2014.

[11] N. M. Spivak, M. E. Schafer, and A. Bystritsky, "Reversible neuroinhibition does not require a thermal mechanism," *Brain Stimul.*, vol. 13, no. 1, p. 262, Jan. 2020.

[12] S. S. Yoo *et al.*, "Focused ultrasound modulates region-specific brain activity," *NeuroImage*, vol. 56, no. 3, pp. 1267–1275, Jun. 2011.

[13] B.-K. Min *et al.*, "Focused ultrasound-mediated suppression of chemically-induced acute epileptic EEG activity," *BMC Neurosci.*, vol. 12, no. 1, p. 23, 2011.

[14] J. Blackmore, S. Shrivastava, J. Sallet, C. R. Butler, and R. O. Cleveland, "Ultrasound neuromodulation: A review of results, mechanisms and safety," *Ultrasound Med. Biol.*, vol. 45, no. 7, pp. 1509–1536, Jul. 2019.

[15] G. Toccaceli, G. Barbagallo, and S. Peschillo, "Low-intensity focused ultrasound for the treatment of brain diseases: Safety and feasibility," *Theranostics*, vol. 9, no. 2, pp. 537–539, 2019.

[16] C. Pasquinelli, L. G. Hanson, H. R. Siebner, H. J. Lee, and A. Thielscher, "Safety of transcranial focused ultrasound stimulation: A systematic review of the state of knowledge from both human and animal studies," *Brain Stimul.*, vol. 12, no. 6, pp. 1367–1380, Nov. 2019.

[17] A. S. Korb *et al.*, "Low-intensity focused ultrasound pulsation device used during magnetic resonance imaging: Evaluation of magnetic resonance imaging-related heating at 3 Tesla/128 MHz," *Neuromodulation*, vol. 17, no. 3, pp. 236–241, Apr. 2014.

[18] L. Ai, J. K. Mueller, A. Grant, Y. Eryaman, and W. Legon, "Transcranial focused ultrasound for BOLD fMRI signal modulation in humans," in *Proc. 38th Annu. Int. Conf. IEEE Eng. Med. Biol. Soc. (EMBC)*, Aug. 2016, pp. 1758–1761.

[19] P. Grolimund *et al.*, "Evaluation of cerebrovascular disease by combined extracranial and transcranial Doppler sonography. Experience in 1,039 patients," *Stroke*, vol. 18, no. 6, pp. 1018–1024, Dec. 1987.

[20] J. H. Kwon *et al.*, "The thickness and texture of temporal bone in brain CT predict acoustic window failure of transcranial Doppler," *J. Neuroimaging*, vol. 16, no. 4, pp. 52–347, Oct. 2006.

[21] K. Barlinn *et al.*, "Exploratory analysis of estimated acoustic peak rarefaction pressure, recanalization, and outcome in the transcranial ultrasound in clinical sonothrombolysis trial," *J. Clin. Ultrasound*, vol. 41, no. 6, pp. 354–360, Jul-Aug. 2013.

[22] K. Hynynen and F. A. Jolesz, "Demonstration of potential noninvasive ultrasound brain therapy through an intact skull," *Ultrasound Med. Biol.*, vol. 24, no. 2, pp. 275–283, Feb. 1998.

[23] A. Bystritsky, A. Korb, J. Stern, and M. Cohen, "Safety and feasibility of focused ultrasound neuromodulation in temporal lobe epilepsy," *J. Therapeutic Ultrasound*, vol. 3, no. S1, p. 27, 2015.

[24] M. M. Monti, C. Schnakers, A. S. Korb, A. Bystritsky, and P. M. Vespa, "Non-invasive ultrasonic thalamic stimulation in disorders of consciousness after severe brain injury: A first-in-man report," *Brain Stimulation*, vol. 9, no. 6, pp. 940–941, Nov. 2016.
[25] F. G. Shellock, T. O. Woods, and J. V. Crues, "MR labeling information for implants and devices: Explanation of terminology," *Radiology*, vol. 253, no. 1, pp. 26–30, Oct. 2009.
[26] M. T. Izatt, D. Lees, S. Mills, C. A. Grant, and J. P. Little, "Determining a reliably visible and inexpensive surface fiducial marker for use in MRI: A research study in a busy Australian radiology department," *BMJ Open*, vol. 9, no. 8, Aug. 2019, Art. no. e027020.
[27] M. E. Schafer and P. A. Lewin, "A computerized system for measuring the acoustic output from diagnostic ultrasound equipment," *IEEE Trans. Ultrason., Ferroelectr., Freq. Control*, vol. 35, no. 2, pp. 9–102, Mar. 1988.
[28] M. E. Schafer, "Techniques of hydrophone calibration," in *Ultrasonic Exposimetry*, M. Ziskin and P. Lewin, eds. Boca Raton, FL, USA: CRC Press, 1993, pp. 217–256.
[29] *Ultrasonics—Hydrophones—Part 2: Calibration for Ultrasonic Fields up to 40 MHz*, document IEC 62127-2:2007 /AMD2:2017, International Electrotechnical Commission, 2017. [Online]. Available: https://webstore.iec.ch/publication/31172
[30] *General Requirements for the Competence of Testing and Calibration Laboratories*, Standard ISO/IEC 17025, International Organization for Standardization, 2018. [Online]. Available: www.iso.org/standard/66912.html
[31] M. E. Schafer, J. Gessert, and W. Moore, "Development of a high intensity focused ultrasound (HIFU) hydrophone system," in *Proc. IEEE Ultrason. Symp.*, Sep. 2005, pp. 1739–1742.
[32] W. Legon, P. Bansal, R. Tyshynsky, L. Ai, and J. K. Mueller, "Transcranial focused ultrasound neuromodulation of the human primary motor cortex," *Sci. Rep.*, vol. 8, no. 1, Jul. 2018, Art. no. 10007.
[33] American Institute of Ultrasound in Medicine. (2017). *Safe Use of Therapeutic Ultrasound*. [Online]. Available: https://www.aium.org/officialStatements/68
[34] United States Food and Drug Administration. (2019). *Marketing Clearance of Diagnostic Ultrasound Systems and Transducers, Guidance for Industry and Food and Drug Administration Staff*. Docket Number FDA-2017-D-5372. [Online]. Available: www.fda.gov/media/71100/download
[35] American Institute of Ultrasound in Medicine. (2015). *Statement on Mammalian Biological Effects of Ultrasound In Vivo*. [Online]. Available: https://www.aium.org/officialStatements/9
[36] American Institute of Ultrasound in Medicine. (2015). *Statement on Mammalian Biological Effects in Tissues Without Gas Bodies*. [Online]. Available: https://www.aium.org/officialStatements/63
[37] T. Deffieux and E. E. Konofagou, "Numerical study of a simple transcranial focused ultrasound system applied to blood-brain barrier opening," *IEEE Trans. Ultrason., Ferroelectr., Freq. Control*, vol. 57, no. 12, pp. 2637–2653, Dec. 2010.
[38] J. L. B. Robertson, B. T. Cox, J. Jaros, and B. E. Treeby, "Accurate simulation of transcranial ultrasound propagation for ultrasonic neuromodulation and stimulation," *J. Acoust. Soc. Amer.*, vol. 141, no. 3, p. 1726, Mar. 2017.
[39] M. A. Samoudi, T. Van Renterghem, and D. Botteldooren, "Computational modeling of a single-element transcranial focused ultrasound transducer for subthalamic nucleus stimulation," *J. Neural Eng.*, vol. 16, no. 2, Apr. 2019, Art. no. 026015.
[40] A. Boutet *et al.*, "The relevance of skull density ratio in selecting candidates for transcranial MR-guided focused ultrasound," *J. Neurosurg.*, vol. 132, no. 6, pp. 1785–1791, May 2019.
[41] J. Stern *et al.*, "Safety of focused ultrasound neuromodulation in humans with temporal lobe epilepsy," *medRxiv*, 2020, doi: 10.1101/2020.04.10.20060855.
[42] N. M. Spivak, "Investigating the effects of focused ultrasound pulsation on cerebral tissue of homo sapiens," B.S. thesis, Dept. Neurosci., UCLA, Los Angeles, CA, USA, 2017.
[43] J. Schindelin *et al.*, "Fiji: An open-source platform for biological-image analysis," *Nature Methods*, vol. 9, no. 7, pp. 676–682, Jun. 28, 2012.
[44] S. S. Yoo, H. Kim, B. K. Min, and S. P. E. Franck, "Transcranial focused ultrasound to the thalamus alters anesthesia time in rats," *Neuroreport*, vol. 22, no. 15, pp. 783–787, Oct. 2011.
[45] D. Coluccia *et al.*, "First noninvasive thermal ablation of a brain tumor with MR-guided focused ultrasound," *J. Therapeutic Ultrasound*, vol. 2, no. 1, p. 17, Dec. 2014.

Mark E. Schafer (Senior Member, IEEE) was born in Pittsburgh, PA, USA. He received the S.B. degree in electrical engineering from the Massachusetts Institute of Technology, Cambridge, MA, USA, in 1979, the M.S. degree in acoustics from Pennsylvania State University, State College, PA, USA, in 1982, and the Ph.D. degree in biomedical engineering from Drexel University, Philadelphia, PA, USA, in 1988.

He is currently the President and Principal Consultant at Sonic Tech, Inc., Ambler, PA, USA, and the Chief Technology Officer of Brainsonix, Inc., Los Angeles, CA, USA. He consults with firms worldwide on design, development, intellectual property, regulatory, and clinical aspects of medical ultrasound products, including diagnostic, therapeutic, and surgical applications. He is a serial entrepreneur and an inventor on 30 patents. He has authored numerous journal articles and book chapters on ultrasound measurement and applications.

Dr. Schafer is a fellow of the American Institute of Ultrasound in Medicine and the Acoustical Society of America. He was a recipient of the Chief's Award for Technology Transfer, U.S. Department of Agriculture and the Past President of the Ultrasonic Industry Association. He is currently the President-Elect of the IEEE UFFC.

Norman M. Spivak was born in Los Angeles, CA, USA, in 1996. He received the B.S. degree in neuroscience from the University of California at Los Angeles (UCLA), Los Angeles, in 2018, where he was elected to the Phi Beta Kappa Society.

Since 2018, he has been a Staff Research Associate with the Department of Neurosurgery and Department of Psychiatry, UCLA. His research interests include invasive and noninvasive techniques of neuromodulation, neuroimaging of psychiatric illness, and consciousness.

Alexander S. Korb was born in Los Angeles, CA, USA, in 1980. He received the B.S. degree in neuroscience from Brown University, Providence, RI, USA, in 2002, and the Ph.D. degree in neuroscience from the University of California at Los Angeles (UCLA), Los Angeles, in 2010, with research on EEG biomarkers of treatment response in major depression.

He then worked as a Staff Research Associate with the Ahmanson-Lovelace Brainmapping Center, UCLA, conducting functional magnetic resonance imaging (fMRI) research. He is currently an Adjunct Assistant Professor with the Department of Psychiatry and Biobehavioral Sciences, UCLA, and the Vice-President of research and development at Brainsonix, Inc., Los Angeles. His research interests include focused ultrasound neuromodulation, neuroimaging of psychiatric illness, and low-tech interventions for improving wellbeing.

Alexander Bystritsky was born in Saint Petersburg, Russia, in 1954. He received the M.D. degree and the Ph.D. degree in psychopharmacology from the Pavlov Medical Institute, Saint Petersburg, in 1977 and 1979, respectively.

He worked as an Associate Researcher with the Department of Psychiatry, New York University, New York City, NY, USA, prior to admission to the NYU-Bellevue Residency Program. Upon completion of his residency in 1985, he moved to the University of California at Los Angeles (UCLA), Los Angeles, CA, USA, as a Robert Wood Johnson Clinical Scholar. He joined the ranks of the faculty in 1987 and remained until his retirement and subsequent recall in 2017. He is currently a Professor Emeritus of psychiatry and biobehavioral sciences with the Jane and Terry Semel Institute for Neuroscience and Human Behavior, UCLA, where he directs the anxiety disorders and targeted brain stimulation programs. He is an inventor of several patents relating to the use of focused ultrasound for brain stimulation. He is the Chief Executive Officer of the Brainsonix Corporation, Los Angeles, the Executive Director of the Tiny Blue Dot Foundation, Santa Monica, CA, USA, and the President of the Institute for Advanced Consciousness Studies, Santa Monica.